Computers and Mathematics with Applications 59 (2010) 1667–1678

Contents lists available at ScienceDirect

Computers and Mathematics with Applications

journal homepage: www.elsevier.com/locate/camwa

Robust path tracking using flatness for fractional linear MIMO systems: A thermal application

Stéphane Victor, Pierre Melchior *, Alain Oustaloup

IMS, UMR 5218 CNRS, Université de Bordeaux - ENSEIRB - ENSCPB, 351 cours de la Libération, F 33405 Talence cedex, France

ARTICLE INFO

Keywords:
Flatness
Path tracking
Fractional differentiation
State-space-like representation
Fractional MIMO systems
Robust control

ABSTRACT

This paper deals with robust path tracking using flatness principles extended to fractional linear MIMO systems. As soon as the path has been obtained by means of the fractional flatness, a robust path tracking based on CRONE control is presented. Flatness in path planning is used to determine the controls to apply without integrating any differential equations when the trajectory is fixed (in space and in time). Several developments have been made for fractional linear SISO systems using a transfer function approach. For fractional systems, especially in MIMO, developments are still to be made. Throughout this paper, flatness principles are applied using polynomial matrices for fractional linear MIMO systems. To illustrate the robustness performances, a third-generation multi-scalar CRONE controller is compared to a PID one.

1. Introduction

Theoretical and experimental studies indicate that thermal [1,2], electrochemical [3] and viscoelastic [4] systems can be defined using non-integer differential equations. Integer models are not appropriate for identifying such systems, unless one applies very complex models.

A new property called flatness characterizing a certain class of non-linear systems, allowing the achievement of a simple and robust control, has been introduced by M. Fliess, J. Levine, Ph. Martin and P. Rouchon (see [5–8]). If we restrict to linear time-invariant systems (LTI), it turns out that such systems are flat if and only if they are controllable and that a particular flat output may be obtained as a by-product of the Brunowsky controllability canonical form. Flat outputs summarize, on their own, all the system dynamics. All system variables will be deduced from them without integrating differential equations.

Expressing the flat output z with the system variables and their time derivatives proves to be more difficult. Flatness is well-suited for trajectory planning and offers the possibility of solving straightforwardly path tracking problems. One point of interest of flatness relies on directly computing the command trajectory, enabling one to generate the desired trajectory without disturbance. In order to reject those disturbances, a robust control strategy is required. Here a third-generation multi-scalar CRONE approach is applied. Then, a comparison with a PID is given through the simulations.

In previous works, the extension of the flatness principle to fractional systems was established in [9–11]. In this paper, the study involves controllable fractional LTI systems control. The originality of this work lies in applying the flatness extensions to a multivariable (MIMO, Multiple-Input–Multiple-Output) fractional system (see [9]), in performing a control strategy for the closed-loop case with a third-generation CRONE controller design and in generating robust path tracking.

The paper is organized as follows. In Section 2, first, some basic facts on fractional differentiation and state-space-like representation are detailed; then, the fractional flatness principles are recalled. The characterization of the so-called

* Corresponding author.
E-mail addresses: stephane.victor@laps.ims-bordeaux.fr (S. Victor), pierre.melchior@laps.ims-bordeaux.fr (P. Melchior), alain.oustaloup@laps.ims-bordeaux.fr (A. Oustaloup).

0898-1221/$ – see front matter © 2009 Elsevier Ltd. All rights reserved.
doi:10.1016/j.camwa.2009.08.008

defining matrices of linear flat outputs and the dynamic inversion of the fractional system are detailed in Section 3. Finally, in Section 4, an application is detailed: the diffusion of two flux densities throughout a metallic rod represents a MIMO fractional system. The next section presents the controller design, and simulations and comparisons are carried out in Section 6, in the presence of disturbances. A conclusion is given in Section 7, recalling the major outlines of this study.

2. State-space-like representation of fractional systems and flatness principles

2.1. Recalling fractional systems

The concept of differentiation to an arbitrary order (non-integer),

$$\mathbf{D}^{\nu} \triangleq \left(\frac{\mathrm{d}}{\mathrm{d}t}\right)^{\nu} \quad \forall \nu \in \mathbb{R}_{+}^{*},$$

was defined in the 19th century by Riemann and Liouville. The ν-order fractional derivative of $x(t)$ is defined as being an integer derivative of order $\lfloor \nu \rfloor + 1$ ($\lfloor . \rfloor$ stands for the floor operator) of a non-integer integral of order $\nu - \lfloor \nu \rfloor$ [12]:

$$\mathbf{D}^{\nu} x(t) = \mathbf{D}^{\lfloor \nu \rfloor + 1} \left(\mathbf{I}^{\lfloor \nu \rfloor + 1 - \nu} x(t)\right) \triangleq \left(\frac{\mathrm{d}}{\mathrm{d}t}\right)^{\lfloor \nu \rfloor + 1} \left(\frac{1}{\Gamma\left(\lfloor \nu \rfloor + 1 - \nu\right)} \int_0^t \frac{x(\tau)\,\mathrm{d}\tau}{(t-\tau)^{\nu - \lfloor \nu \rfloor}}\right), \tag{1}$$

where $t > 0$, $\forall \nu \in \mathbb{R}_{+}^{*}$, and the Euler's Γ function is defined as

$$\Gamma(x) = \int_0^{\infty} e^{-t} t^{x-1} \mathrm{d}t \quad \forall x \in \mathbb{R}^{*} \setminus \mathbb{N}^{-}. \tag{2}$$

In its most general form, a monovariable fractional model can be defined by a differential equation characterized with its derivation orders that can be real (integer or fractional):

$$a_0 \mathbf{D}^{\nu_{a_0}} y(t) + a_1 \mathbf{D}^{\nu_{a_1}} y(t) + \cdots + a_L \mathbf{D}^{\nu_{a_L}} y(t) = b_0 \mathbf{D}^{\nu_{b_0}} u(t) + \cdots + b_M \mathbf{D}^{\nu_{b_M}} u(t), \tag{3}$$

where $\mathbf{D}$ is the derivative operator. Let us consider that $\nu_{a_i} < \nu_{a_j}$ for $0 \leq i < j \leq L$ and that $\nu_{a_p} < \nu_{b_q}$ for $0 \leq p < q \leq M$.

Definition. The commensurate order is defined as the greatest real positive divisor of the derivative orders $(\nu_{a_1}, \ldots, \nu_{a_n}, \nu_{b_0} \ldots \nu_{b_m})$ in (3) (the highest number is generally chosen).

For integer systems, the commensurate order is equal to 1. For real non-commensurate differentiation order, using an order approximation by rational numbers, it is possible to determine a common divisor order ν.

In the following, all fractional systems considered are supposed to be of commensurate order.

2.2. State-space-like representation

Elementary differential equations in which the order is subjected to two levels of generalization (see [13] for details) appear in the extension of the state-space representation for fractional linear systems (see [13–16]). In a classic state-space representation, the state needs only its previous value in order to predict the next step; however, in fractional calculus, the fractional derivative needs the whole past of the state to predict its next value [17,18]. Consequently, in fractional calculus, this representation is called a "fractional" or state-space-"like" representation. In this paper, only the first level of generalization is considered[1]; the derivation orders of each elementary differential equation are the same and given by the commensurate order, which is a scalar,

$$\begin{cases} x^{(\nu)}(t) = Ax(t) + Bu(t) \\ y(t) = Cx(t) + Du(t), \end{cases} \tag{5}$$

where A, B, C and D are respectively $n \times n$, $n \times m$, $r \times n$ and $r \times m$ constant matrices.

[1] In the second level of generalization, the derivation orders of the elementary differential equations are different, and the system takes the following representation:

$$\begin{cases} x^{(\underline{\nu})}(t) = Ax(t) + Bu(t) \\ y(t) = Cx(t) + Du(t), \end{cases} \tag{4}$$

where $\underline{\nu} = (\nu_1, \ldots, \nu_K)^{\mathrm{T}}$, $\nu_{i=1,\ldots,K} \in \mathbb{R}_{+}$. The state variable of rank i is differentiated at the order ν_i. For reasons of simplicity, the study will proceed for a first level of generalization, with a scalar ν.

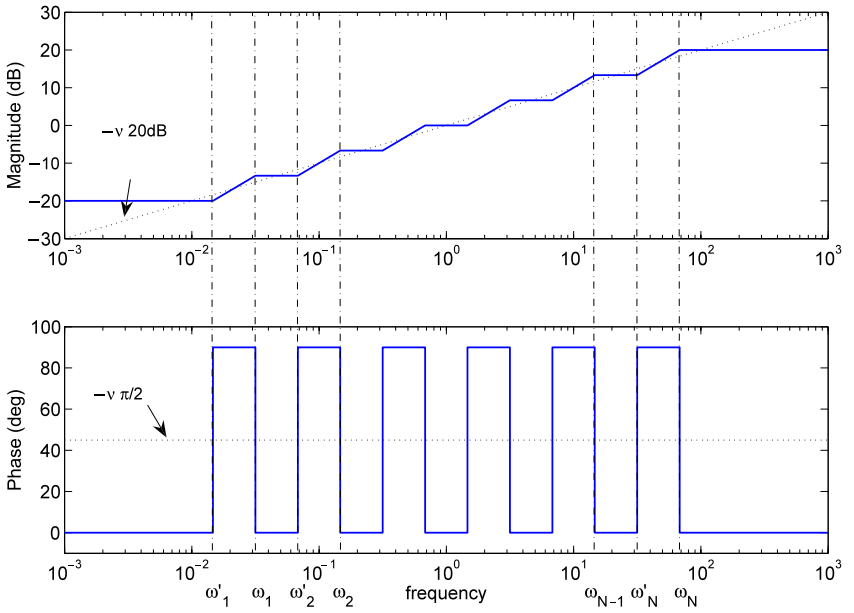

Fig. 1. Recursive approximation of a fractional differentiator with poles and zeros.

2.3. Temporal simulation of fractional differentiation systems

The proposed approach works with any simulation algorithm for fractional differentiation systems in the time domain. However, only the simulation algorithm used in the example of this paper is explained here, as the objective is not to discuss different simulation algorithms.[2] Due to the consideration that real physical systems generally have band limited fractional behavior and due to the practical limitations of input and output signals (Shannon's cut-off frequency for the upper band and the spectrum of the input signal for the lower band), fractional operators are usually approximated by high integer order models. As a result, a fractional model and its integer approximation have the same dynamics within a frequency band limit. The most commonly used approximation for s^ν in the frequency band $[\omega_A, \omega_B]$ is the recursive distribution of zeros and poles proposed in [13] (see Fig. 1):

$$s^\nu \to s^\nu_{[\omega_A,\omega_B]} = C_0 \left(\frac{1 + \frac{s}{\omega_A}}{1 + \frac{s}{\omega_B}} \right)^\nu \approx C_0 \prod_{k=1}^{N} \frac{1 + \frac{s}{\omega'_k}}{1 + \frac{s}{\omega_k}} \tag{6}$$

where $\omega_i = \alpha\omega'_i$, $\omega'_{i+1} = \eta\omega'_i$ and

$$\gamma = 1 - \frac{\log\alpha}{\log\alpha\eta}, \tag{7}$$

and α and η define the differentiation order γ. The bigger N the better the approximation of the differentiator s^ν.

3. Fractional flat output of a fractional linear system stemming from a polynomial form

Throughout this paper, $u^{(k)}$ stands for the kth-order derivative of u with respect to time, k being a non-integer scalar, and each component of u is derived at order k. Let the system be given by the following differential equation:

$$x^{(\nu)} = f(x, u), \tag{8}$$

with $x \in \mathbb{R}^n$, $u \in \mathbb{R}^m$ being the input command, $\nu \in [0, 2]$[3] and $f = (f_1, \ldots, f_n)$ a regular function of x and u where the rank of $\frac{\partial^\nu f}{\partial u^\nu}$ is equal to m.

This system is said to be differentially flat (see [5] for the rational case and [10] for the extension to fractional systems and its algebra of s^ν-polynomials) if one can find a set of independent variables referred to as the flat output z such that each

2 Refer to [19], for an extended discussion on time-domain simulation of fractional differentiation systems.

3 It is proved in [20] that fractional differentiation systems are unstable for a commensurable order $\nu \notin]0, 2[$.

system variable, including the inputs, is a function of z and a finite number of its time derivatives. The fractional flat output z is such that

$$z = h(x, u, u^{(\nu)}, u^{(2\nu)}, \ldots, u^{(\beta\nu)}), \quad z \in \mathbb{R}^m, \tag{9}$$

with β a finite m-tuple of integers [4] and ν stands for the commensurable order.

3.1. Fractional flat output of a fractional linear system

In the following, the Laplace transformation $\mathscr{L}$, which is an algebraic tool generally used to represent fractional differentiation systems, is defined by (see [21,18]):

$$\mathscr{L}\{\mathbf{D}^{\gamma} x(t)\} = s^{\gamma} X(s) \quad \text{if } x(t) = 0 \quad \forall t \leq 0. \tag{10}$$

All variables are in the operational domain; in order to get back to the time domain, the Laplace inverse operator $\mathscr{L}^{-1}$ should be applied. Fractional linear systems such as (5) can be rewritten in the following polynomial matrix representation:

$$\begin{cases} A(s^{\nu})X = BU \\ Y = CX + DU, \end{cases} \tag{11}$$

with $A(s^{\nu}) = s^{\nu} I - A$ an $n \times n$ matrix whose entries are polynomials of the formal variable s^{ν} (I being the identity matrix), B, C and D constant matrices, and X, U and Y the Laplace transforms of x, u and y respectively. System (11) is assumed controllable, i.e. A and B are left coprime (see [7]).

A *fractional linear flat output* defines an output defined by (9) with h being linear; the state variables, the input command and the output can be redefined with z as

$$\begin{aligned} x_i &= \sum_{j=1}^{m} \sum_{k=0}^{\alpha_j} a_{i,j,k} z_j^{(k\nu)}, \quad i = 1, \ldots, n, \\ u_l &= \sum_{j=1}^{m} \sum_{k=0}^{\alpha_j+1} b_{l,j,k} z_j^{(k\nu)}, \quad l = 1, \ldots, m, \\ y_q &= \sum_{j=1}^{m} \sum_{k=0}^{\sigma_j} c_{q,j,k} z_j^{(k\nu)}, \quad q = 1, \ldots, r, \end{aligned} \tag{12}$$

where $\underline{\alpha}$ and $\underline{\sigma}$ are m-tuples of integers. Notice that all differentiation orders are multiples of the commensurate order ν.

In the polynomial matrix language, (12) reads

$$X = P(s^{\nu}) Z, \qquad U = Q(s^{\nu}) Z, \tag{13}$$

where P (resp. Q) is an $n \times m$ (resp. $m \times m$) polynomial matrix of s^{ν}, with entries $P_{i,j}(s^{\nu}) = \sum_{k=0}^{q_j} a_{i,j,k} s^{\nu_{i,k}}$ (resp. $Q_{l,j}(s^{\nu}) = \sum_{k=0}^{q_j+1} b_{l,j,k} s^{\nu_{l,k}}$). For an overview of s^{ν}-polynomial algebra, refer to [10].

Matrices P and Q satisfying (13) are called defining matrices of the fractional flat output z.

Theorem. *The variable $z = (z_1, \ldots, z_m)$ is a linear flat output of system (11) if and only if its defining matrices P and Q are given by*

$$\begin{aligned} &R^{\mathrm{T}} A(s^{\nu}) P(s^{\nu}) = 0, \\ &A(s^{\nu}) P(s^{\nu}) = BQ(s^{\nu}), \end{aligned} \tag{14}$$

with R an arbitrary matrix of rank $n - m$ orthogonal to B (this means that $R^{\mathrm{T}} B = 0$), and with $P(s^{\nu})$ and $Q(s^{\nu})$ of rank m for every s^{ν} and right coprime[5].

In addition, the linear flat output y of the controllable system (11) always exists (and therefore its defining matrices P and Q always exist too).

[4] For an m-tuple of integers $\beta = (\beta_1, \ldots, \beta_m)$ of dimension m and a vector u of dimension m, the notation $u^{(\beta)}$ denotes $\left(u^{(\beta_1)}, \ldots, u^{(\beta_m)}\right)$.

[5] For the proof for fractional systems, one may refer to [10].

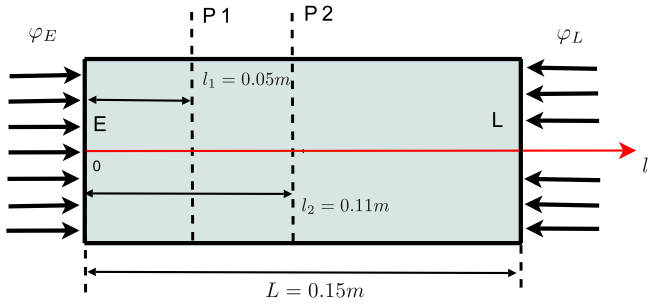

Fig. 2. Finite metallic rod, under the influence of two thermal fluxes on each end. Two measures are taken, at P_1 ($l = l_1$) and P_2 ($l = l_2$).

3.2. Dynamic inversion of a fractional differentiation system

Once the state variable x (resp. the input command u) has been expressed using the flat output z with its defining matrix P (resp. Q), the desired output y_{des} can be expressed using the fractional flat output z. Knowing y_{des}, the fractional differentiation system is inverted in order to get the fractional flat output.

From (5) and (13), the desired output is expressed using the fractional flat output as

$$Y_{des} = \left(CP\left(s^{\nu}\right) + DQ\left(s^{\nu}\right)\right) Z. \tag{15}$$

Thus, in order to have a desired output, it is necessary to invert (15) in order to determine the flat output entirely. We write $W(s^{\nu}) = CP(s^{\nu}) + DQ(s^{\nu})$ which is of dimension $r \times m$.

(1) *If* $r = m$ *and* $rank(W) = m$, W is invertible, and the flat output is easily determined as

$$Z = W^{-1} Y_{des}. \tag{16}$$

(2) *If* $r < m$, W is left invertible (the pseudo-inverse is used here), and the flat output can be expressed as

$$Z = \left(W^{\mathrm{T}} W\right)^{-1} W^{\mathrm{T}} Y_{des}. \tag{17}$$

(3) *If* $r > m$, in this case, the system has more outputs than input commands. Some outputs are linear combinations of independent outputs or linear combinations of the command inputs. After isolating those outputs, the system can be brought to one of the two previous cases.

4. Application: Thermal system

4.1. Description of the thermal application

In this section, a MIMO fractional system will be handled using a fractional state-space-like representation: a finite dimensional thermal system is considered. [1,22] established that the thermal flux throughout a metallic bar can be defined with fractional differential equations. The thermal system is constituted by a long aluminium rod of $L = 0.15$ m heated by two resistors, one on each end of the bar. It is considered as a homogeneous finite plane medium with conductivity $\lambda = 10$ W m^{-1} K^{-1}, with diffusivity $\alpha = 10^{-5}$ m^2 s^{-1} and initially at 0 °C. The entire surface of the rod is assumed to be insulated in order to ensure a unidirectional heat transfer. Losses on the surface where the thermal flux is applied are neglected. The aim here is to control the temperature at two specific points of the rod, measured at distances of $l_1 = 0.05$ m and $l_2 = 0.11$ m from one of the heated ends (Fig. 2), knowing that the rod is subjected to two different heat flux densities.

The non-integer physical behavior proof of this system and the calculation details are not given here as they were already developed in [10]. The model linking the flux density applied on the outgoing normal surface of the medium to the temperature measured at an abscissa l_n ($n = 1$ for l_1, $n = 2$ for l_2) inside the medium is given by the following transfer function (resulting from the theorem of superposition as the system is supposed linear):

$$H\left(l_n, s\right) = H_E\left(l_n, s\right) + H_L\left(l_n, s\right), \tag{18}$$

with the following definitions:

- $$H_E(l_n, s) = \frac{T_E(l_n, s)}{S\varphi_E(0, s)} = \frac{\sum_{k=0}^{K} b_k s^{k\nu}}{\sum_{k=1}^{K} a_k s^{(k+1)\nu}} \tag{19}$$

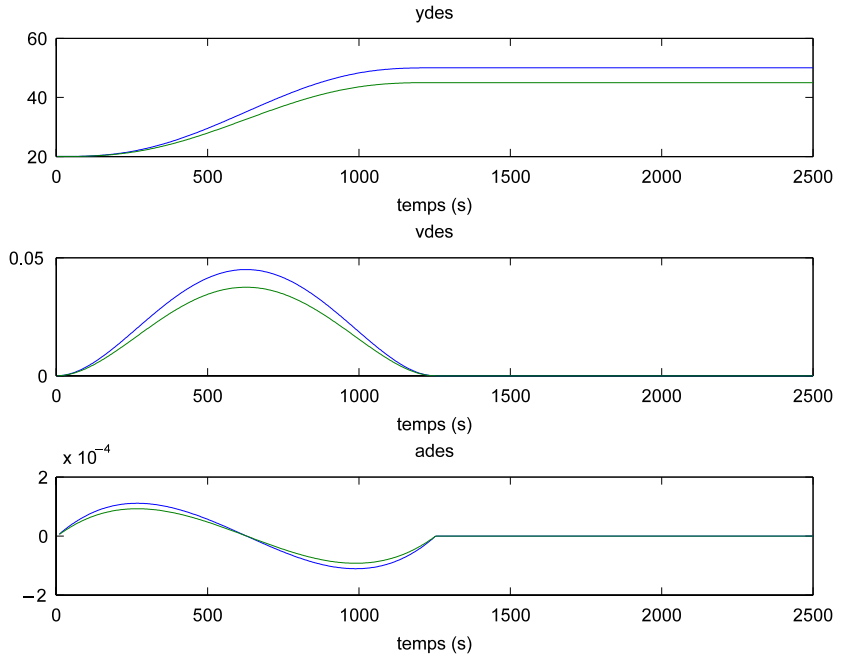

Fig. 3. Desired temperature and its time derivatives.

where $S = \pi R_{bar}^2$ is the bar section, $\varphi_E(l = 0, s)$ is the flux density coming from $l = 0$ (at point E on Fig. 2) and $T_E(l, s)$ the temperature resulting from $l = 0$ measured at point P_n ($l = l_n$; Fig. 2), $\nu = 0.5$ is the commensurable order, $b_k = \frac{(2L-l_n)^k + l_n^k}{k!\alpha^{k/2}}$ and $a_k = S\lambda \frac{(2L)^k}{k!\alpha^{\frac{k+1}{2}}}$.

- $$H_L(l_n, s) = \frac{T_L(l_n, s)}{S\varphi_L(L, s)} = \frac{\sum_{k=0}^{K} b'_k s^{k\nu}}{\sum_{k=1}^{K} a'_k s^{(k+1)\nu}} \tag{20}$$

where $\varphi_L(l = L, s)$ is the flux density coming from $l = L$ (at point L on Fig. 2) and $T_L(l, s)$ the temperature resulting from $l = L$ measured at point P_n ($l = l_n$; Fig. 2), $b'_k = \frac{(L+l_n)^k + (L-l_n)^k}{k!\alpha^{k/2}}$ and $a'_k = S\lambda \frac{(2L)^k}{k!\alpha^{\frac{k+1}{2}}}$.

Thus, the fractional state-space-like representation is as follows:

$$A = \begin{bmatrix} 0 & 1 & 0 & & & \\ \vdots & & \ddots & & 0 & \\ 0 & & & 1 & & \\ -a_0 & \cdots & -a_k & \cdots & -a_K & \\ & & & 0 & 1 & 0 \\ & 0 & & \vdots & & \ddots \\ & & & 0 & 0 & 1 \\ & & & -a'_0 & \cdots -a'_k & \cdots -a'_K \end{bmatrix},$$

$$B = \begin{bmatrix} 0 & \cdots & 1 & 0 & \cdots & 0 \\ 0 & \cdots & 0 & 0 & \cdots & 1 \end{bmatrix}^{\mathrm{T}}, \tag{21}$$

$$C = \begin{bmatrix} b_{1,0} & \cdots & b_{1,K} & b'_{1,0} & \cdots & b'_{1,K} \\ b_{2,0} & \cdots & b_{2,K} & b'_{2,0} & \cdots & b'_{2,K} \end{bmatrix},$$

$$D = 0.$$

The metallic rod will have to rise 30 °C above the initial temperature in 1250 s at P_1, and 25 °C above in P_2 (see Figs. 3 and 4) and will stabilize for the same period of time, according to the following chosen path, a Polynomial Interpolation of

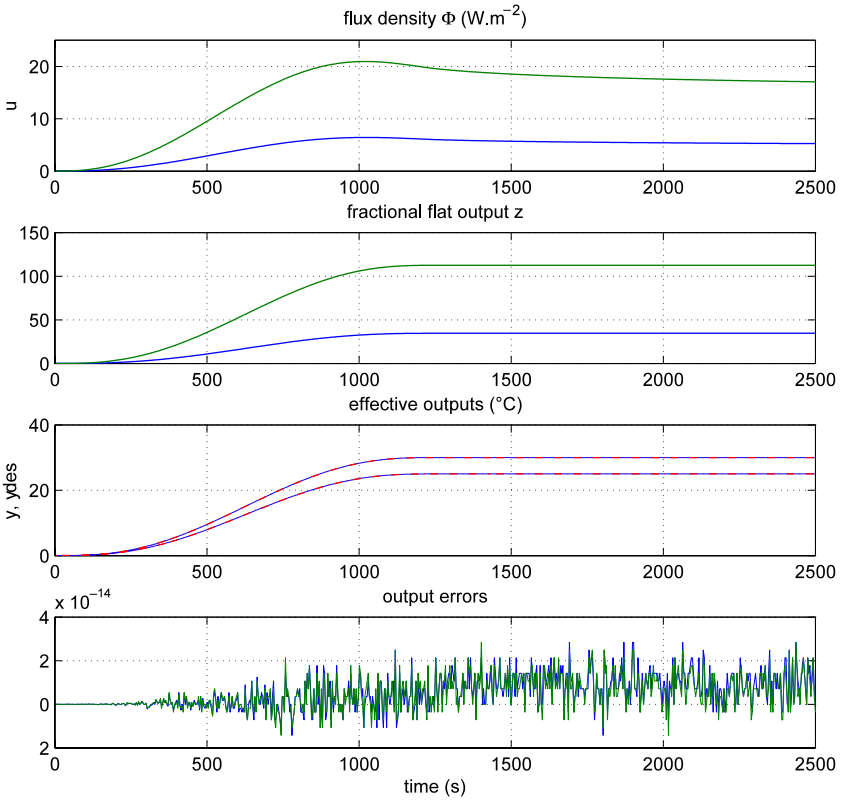

Fig. 4. Simulation of the metallic rod in open loop: input commands ($u = \Phi$), flat outputs, desired (dashed) and effective outputs, and the output errors.

degree 5 (PI5):

$$y_n(t) = q_i + 80\left(q_{f,n} - q_i\right)\frac{t^3}{t_f^3} - 240\left(q_{f,n} - q_i\right)\frac{t^4}{t_f^4} + 192\left(q_f - q_i\right)\frac{t^5}{t_f^5}, \tag{22}$$

with $q_i = 0\ ^\circ C$, $q_{f,n=1} = 30\ ^\circ C$, $q_{f,n=2} = 25\ ^\circ C$, and $t_f = 2500$ s.

Here, the PI5 path is such that the first and second derivatives of the temperature are equal to zero at the initial and final temperatures (Fig. 3).

4.2. Control algorithm test in the open loop

The fractional flat output has been computed with $Z = W^{-1}Y_{des}$, and the input commands and outputs are illustrated in Fig. 4. An algorithm able to generate flat outputs and the input commands, in order to get the chosen paths, has been created for fractional MIMO systems. The control calculated in this way is used in the simulation to provide an off-line computed control for a thermal testing bench. The third graph of Fig. 4 shows that the effective outputs obtained with the input commands (the first graph of Fig. 4) are noticeably the same as the chosen path.

5. Controller design

According to the fractional state-space-like representation (21), as the system considered is decoupled, the regulators can be computed separately in a multi-scalar approach. Several fractional control design exist in the literature [23–26]; here, a third-generation Crone controller is adopted. Two regulators are computed, one for each input command. For a better comparison, two types of controller are given: a PID and a CRONE controller. In the following the index E stands for the incoming flux from $l = 0$, and L stands for the incoming flux from $l = L$ (see Fig. 2), and X stands for both E and L. The controllers should assure a robustness to disturbances and to parametric uncertainties, which bring about gain and phase variations. A variation on R_{bar} influences the gain of the plant: the lower R_{bar} is, the higher the gain will be; a variation of λ brings about a phase variation: the lower λ is, the higher the phase variation will be. Fig. 5 shows the nominal plant and the envelopes due to uncertain parameters.

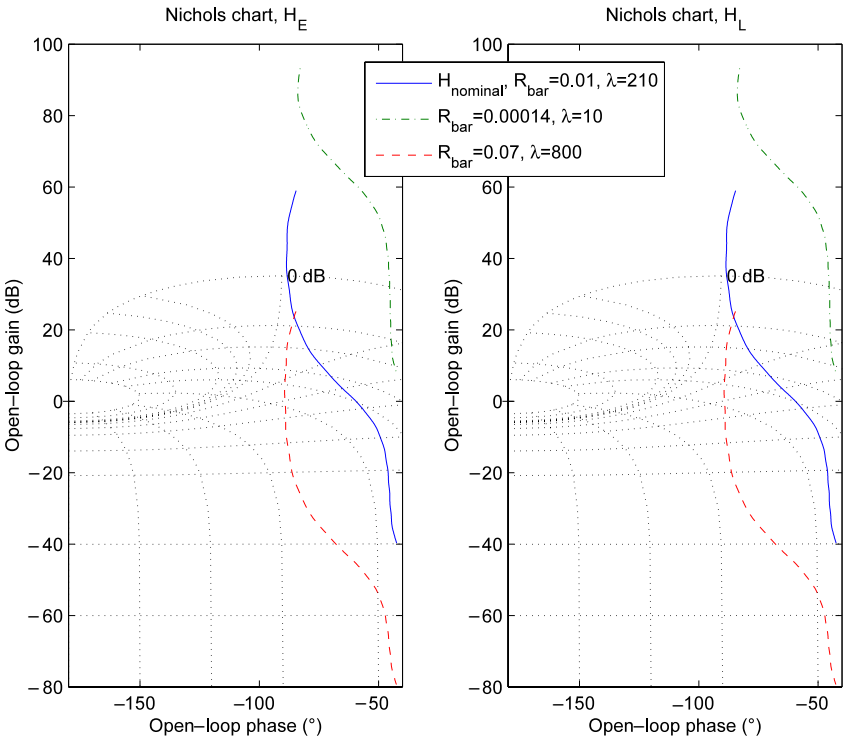

Fig. 5. Nichols diagram of the thermal plant with its uncertainties (left for H_E, right for H_L); nominal in blue, extreme envelopes dashed. (For interpretation of the references to colour in this figure legend, the reader is referred to the web version of this article.)

5.1. The PID controller design

The PID (Proportional Integral Differential) controllers are designed for a desired open-loop gain crossover frequency $\omega_{cg,X} = 0.3$ rad/s. A phase margin of 45° is chosen in order to reduce the overshoot. All of these specifications lead to the PID controller described by the following transfer function explaining the proportional, integral, differential and filtering (to reduce noise in high frequencies) action parts ($X = E, L$):

$$C_X(s) = C_{o,X}\left(\frac{1+\frac{s}{\omega_{i,X}}}{\frac{s}{\omega_{i,X}}}\right)\left(\frac{1+\frac{s}{\omega_{a,X}}}{1+\frac{s}{\omega_{b,X}}}\right)\left(\frac{1}{1+\frac{s}{\omega_{f,X}}}\right)$$
$$C_{o,E} = 18.07, \quad \omega_{i,E} = 0.2, \quad \omega_{a,E} = 0.86,$$
$$\omega_{b,E} = 0.06, \quad \omega_{f,X} = 2, \tag{23}$$
$$C_{o,L} = 18.85, \quad \omega_{i,L} = 0.23, \quad \omega_{a,L} = 0.86,$$
$$\omega_{b,L} = 0.06, \quad \omega_{f,X} = 2.3.$$

Fig. 6 shows the open-loop case with the PID controller in the Nichols diagram considering the uncertainties.

5.2. The CRONE controller design

The CRONE controller (the name derives from a French acronym for fractional order robust control (see [27])) is defined within the frequency range $[\omega_A, \omega_B] = [0.001, 1]$ rad/s around the desired open-loop gain crossover frequency $\omega_{cg,X}$ in order to ensure a constant phase and more particularly to ensure small variations of the closed-loop system stability degree. The aim of the CRONE control system design (CSD) is to find a diagonal open-loop transfer matrix whose elements are fractional order transfer functions. It is parameterized to achieve a perfect decoupling for the nominal plant, accuracy specifications at low frequencies, required nominal stability margins of the closed loops (behaviors around the required cut-off frequencies), and specifications of all the control efforts at high frequencies. After an optimization of the diagonal open-loop $\beta_{0,X}(s)$ transfer matrix, frequency-domain system identification is carried out to obtain the fractional controller. Open-loop transfer functions are used to satisfy the objectives specified above. For a detailed overview of the third-generation Crone controller, readers may refer to [28].

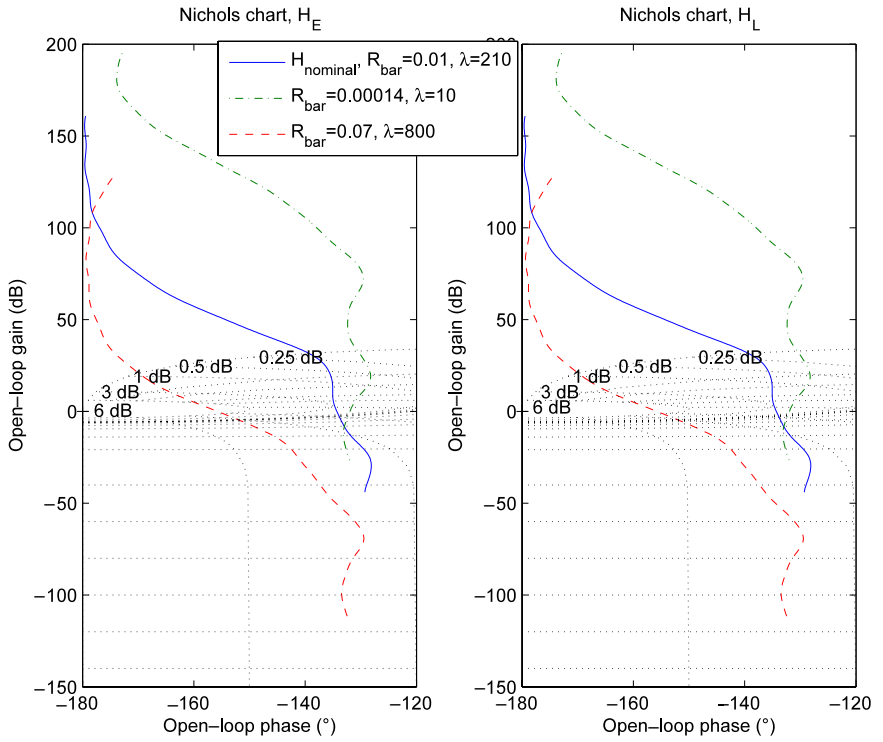

Fig. 6. Nichols diagram of the open loop with PID (left for H_E, right for H_L); nominal in blue, extreme envelopes dashed. (For interpretation of the references to colour in this figure legend, the reader is referred to the web version of this article.)

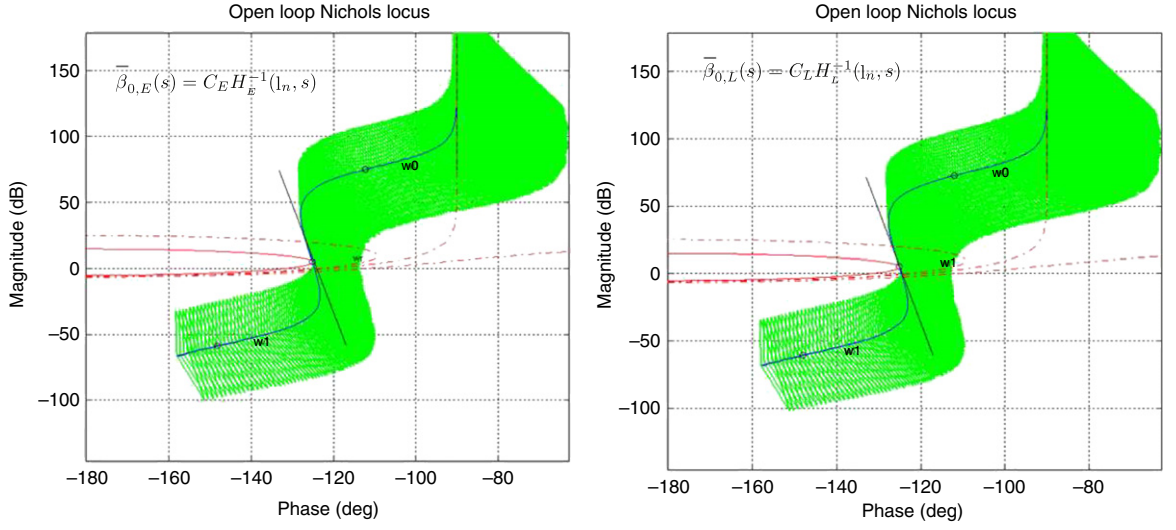

Fig. 7. Nichols diagram of the fractional open loop considering gain ($[0.02 - 50]$) and phase ($12°$–$25°$) uncertainties.

The open-loop transfer function can be described as based on band limited complex non-integer integration:

$$\beta_{0,X}(s) = C_X^{\mathrm{sign}(b)} \left(\frac{1 + s/\omega_{\mathrm{h,X}}}{1 + s/\omega_{\mathrm{l,X}}}\right)^{a} \left(\Re e_{/\mathrm{i}} \left\{ \left(C_{\mathrm{g}} \frac{1 + s/\omega_{\mathrm{h,X}}}{1 + s/\omega_{\mathrm{l,X}}} \right)^{\mathrm{i}b} \right\}\right)^{-q\,\mathrm{sign}(b)} \tag{24}$$

with $C_X = \cosh\left[b_X \left(\arctan\left(\frac{\omega_{\mathrm{cg,X}}}{\omega_{\mathrm{l,X}}}\right) - \arctan\left(\frac{\omega_{\mathrm{cg,X}}}{\omega_{\mathrm{h,X}}}\right)\right)\right]$ and $C_{\mathrm{g,X}} = \left(\frac{1+\left(\frac{\omega_{\mathrm{cg,X}}}{\omega_{\mathrm{l,X}}}\right)^2}{1+\left(\frac{\omega_{\mathrm{cg,X}}}{\omega_{\mathrm{h,X}}}\right)^2}\right)^{1/2}$.

The corner frequencies are placed around the extreme frequencies of the frequency range considered such that $\omega_{\mathrm{l,X}} < \omega_{\mathrm{A}} < \omega_{\mathrm{cg,X}} < \omega_{\mathrm{B}} < \omega_{\mathrm{h,X}}$.

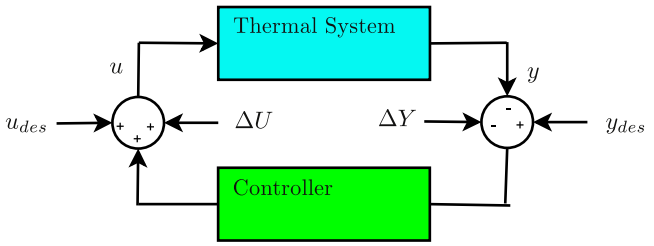

Fig. 8. Closed-loop control scheme.

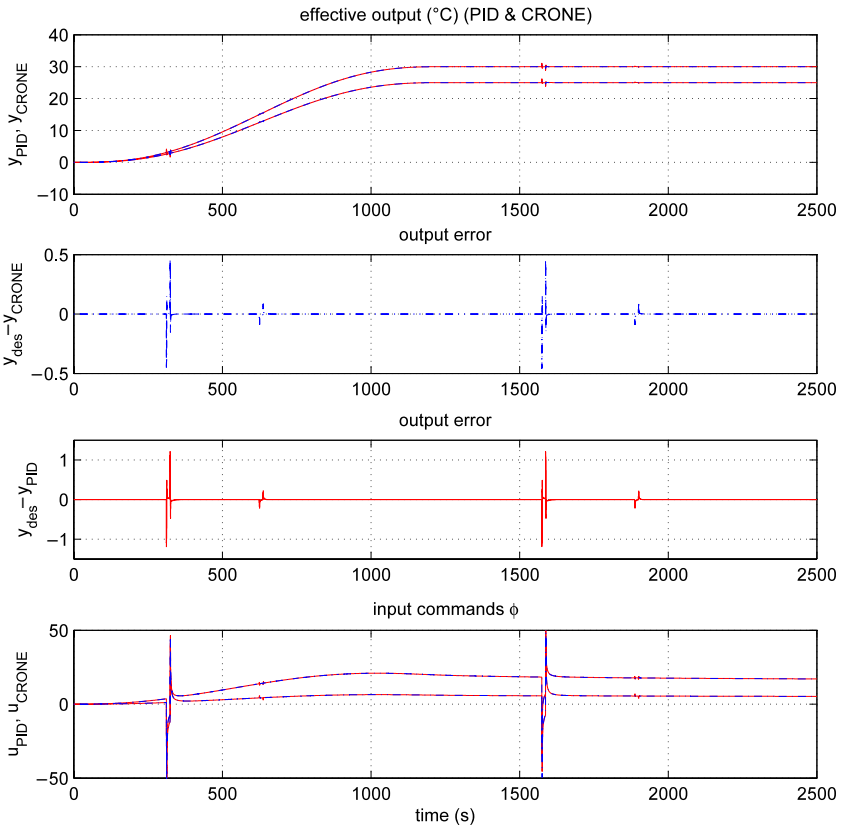

Fig. 9. Simulation of the nominal plant; measured temperature (CRONE dashed, PID red), output error $y_{CRONE}-y_{des}$, output error $y_{PID}-y_{des}$, input commands Φ. (For interpretation of the references to colour in this figure legend, the reader is referred to the web version of this article.)

For a stable and minimum phase plant, the generalized template is taken into account in the open-loop transfer function as follows:

$$\bar{\beta}_{0,X}(s) = \beta_{l,X}(s)\,\beta_{0,X}(s)\,\beta_{h,X}(s) \tag{25}$$

with $\beta_{l_X}(s) = C_{l_X}\left(\frac{\omega_{l_X}}{s}+1\right)^{n_{l_X}}$, the order n_{l_X} fixing the accuracy of each closed loop, and $\beta_{h_X}(s) = \frac{C_{h_X}}{\left(\frac{s}{\omega_{h_X}}+1\right)^{n_{h_X}}}$, the order n_{h_X} enabling the elements of the controller to be proper. Remark that the desired open-loop gain crossover frequencies $\omega_{cg,X}$ are almost the same. This third-generation CRONE control open-loop transfer function has been defined using the gain crossover open-loop frequency and by inverting the plant as follows:

$$\begin{aligned} &C_X = \overline{\beta}_{0,X}(s)H_X^{-1}(l_n, s)\\ &\omega_{l,X} = 10^{-3}\ \text{rad s}^{-1}, \qquad \omega_{h,X} = 10^{3}\ \text{rad s}^{-1}, \qquad \omega_{r,X} = 0.3\ \text{rad s}^{-1},\\ &\gamma = a + ib = 1.24 - 0.11i, \qquad n_{l,X} = 1.5, \qquad n_{h,X} = 2. \end{aligned} \tag{26}$$

The computations are to ensure stability for gain uncertainties between 0.02 and 50, and for phase uncertainties between 12.5° and 25°. Fig. 7 presents the open loop in the Nichols diagram considering the uncertainties.

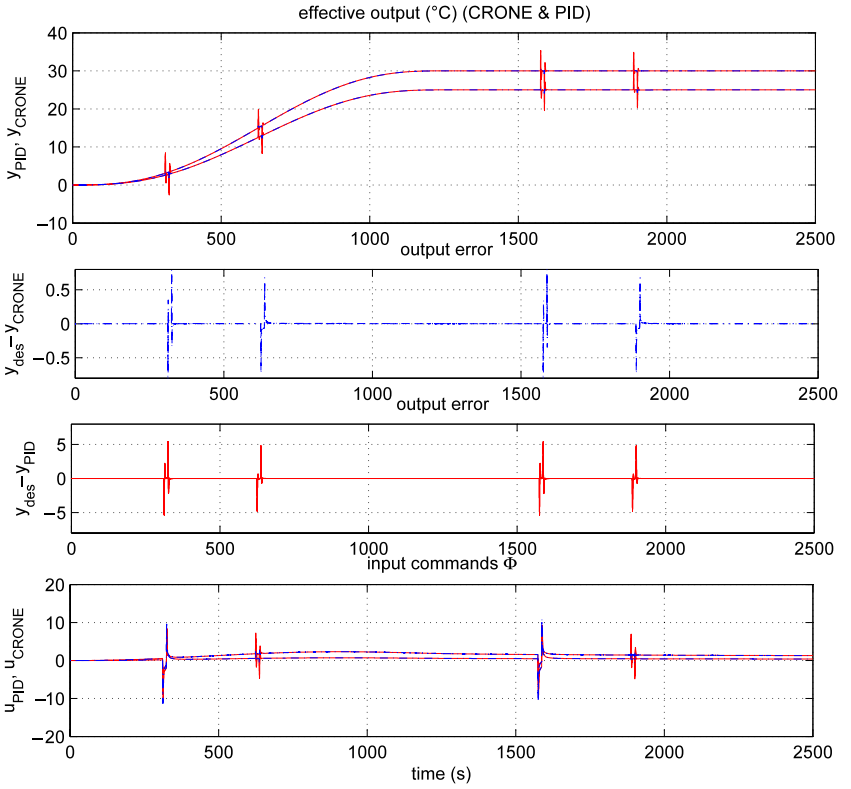

Fig. 10. Simulation with $50 \times H$; measured temperature (CRONE dashed, PID red), output error $y_{CRONE} - y_{des}$, output error $y_{PID} - y_{des}$, input commands Φ. (For interpretation of the references to colour in this figure legend, the reader is referred to the web version of this article.)

6. Simulation results

The system is studied in the closed-loop case so as to measure its immunity to different disturbances applied to its input ΔU and to its output ΔY. The control scheme is presented in Fig. 8, with U_{ref} the control obtained by the flatness principle using the chosen reference trajectory y_{des} (the desired output). The PID and Crone controllers are both used in the simulation. For this, the disturbances and gain variation influence on the path tracking are studied. Two control input disturbances of 35 s are applied: one at 625 s (during the ascension) and another one at 1910 s during the constant phase. Moreover, two output disturbances of 35 s are applied: one at 312 s (during the ascension) and another one at 1600 s during the constant phase. Time responses are given for different gain variations (1, 0.02 and 50 times the gain). It is recalled that the controllers have the same desired open-loop gain crossover frequency. Fig. 9 shows a better performance of the CRONE controller compared to the PID one. Simulations with the nominal plant show similar disturbance rejection as regards the time responses (3 s); however the overshoot is higher for the PID: almost 2 times higher. The robustness study is presented in figure Fig. 10. The CRONE controller show the same sensitivity as regards time responses and disturbance rejection. It is 2 times quicker (3.5 s instead of 7 s) and the output error is 10 times lower. A better path tracking performance with the CRONE controller can be accomplished in the presence of disturbances and gain and phase variations. A more detailed synthesis presentation of a CRONE third-generation controller for MIMO systems can be carried out. The authors recommend to the following references: [29] for the CRONE command, [28] for MIMO fractional controller design.

7. Conclusion and outlook

A new path tracking design combining flatness, fractional MIMO systems and CRONE control approaches was presented. First of all, the flatness principle definitions and the fractional state-space-like representation used in control theory are recalled. After that, using the polynomial matrix form, the flat output is computed after the dynamic inversion of the fractional system. Then, this method is applied to a fractional MIMO system: a rod was subjected to two different flux densities, one at each end, in order to control the temperature at two specific points of the rod. Variations of R_{bar} and λ introduce gain and phase uncertainties that the control strategy should consider. The study of robust path tracking via a third-generation CRONE control was integrated. To show the performance of the CRONE controller, simulations with two different controllers (PID and CRONE) were implemented. These simulations clearly indicated the robustness of the path tracking strategy for the CRONE controller, in terms of sensitivity, disturbance rejection and time responses.

Furthermore, this study could be extended to non-linear fractional systems. Much more research on this topic remains to be done for fractional systems, such as non-linear fractional systems, and the extension of flatness principles for such systems.

References

[1] J.-L. Battaglia, L. Le Lay, J.-C. Batsale, A. Oustaloup, O. Cois, Heat flux estimation through inverted non integer identification models, Int. J. Thermal Science 39 (3) (2000) 374–389.
[2] L. Dorcak Petras, I.B. Vinagre, V. Feliu, Fractional digital control of a heat solid: Experimental results, in: Proceedings of International Carpathian Control Conference ICCC'02, page 365–370, 2002.
[3] R. Darling, J. Newman, On the short behavior of porous intercalation electrodes, J. Electrochem. Soc. 144 (9) (1997) 3057–3063.
[4] X. Moreau, C. Ramus-Serment, A. Oustaloup, Fractional differentiation in passive vibration control, Nonlinear Dynam. 29 (1–4) (2002) 343–362. Special Issue on "Fractional Order Calculus and its Applications".
[5] M. Fliess, J. Lévine, PH. Martin, P. Rouchon, Flatness and defect of nonlinear systems: introductory theory and examples, Internat. J. Control 61 (1995) 1327–1361.
[6] M. Fliess, J. Lévine, Ph. Martin, P. Rouchon, A Lie–Bäcklund approach to equivalence and flatness of nonlinear systems, IEEE Trans. Autom. Control 44 (1999) 922–937.
[7] J. Levine, D.V. Nguyen, Flat output characterization for linear systems using polynomial matrices, Syst. Control Lett. 48 (2003) 69–75.
[8] L. Bitauld, M. Fliess, J. Lévine, A flatness based control synthesis of linear systems and application to windshield wipers, in: ECC'97, Brussels, 1997.
[9] S. Victor, P. Melchior, A. Oustaloup, Flatness principle extension to linear fractional MIMO systems: Thermal application, in: The 14th IEEE Mediterranean Electrotechnical Conference (MELECON'08), Ajaccio, France, May, IEEE, 2008.
[10] S. Victor, P. Melchior, A. Oustaloup, Extension de la platitude aux systèmes fractionnaires MIMO: Application à un système thermique, in: CIFA'08, Bucarest, Roumania, September 2008.
[11] P. Melchior, M. Cugnet, J. Sabatier, A. Poty, A. Oustaloup, Flatness control of a fractional thermal system, in: J. Sabatier, O.P. Agrawal, J.A. Tenreiro Machado (Eds.), Advances in Fractional Calculus Theoretical Developments and Applications in Physics and Engineering, Springer, 2007, pp. 493–509. (chapter VII).
[12] S.G. Samko, A.A. Kilbas, O.I. Marichev, Fractional integrals and derivatives: Theory and applications, Gordon and Breach Science, 1993.
[13] A. Oustaloup, La dérivation non-entière, Hermès, Paris, 1995.
[14] D. Matignon, Représentations en variables d'état de modèles de guides d'ondes avec dérivation fractionnaire, PhD thesis, Université de Paris-Sud, Orsay, 1994.
[15] J.-C. Trigeassou, T. Poinot, J. Lin, A. Oustaloup, F. Levron, Modeling and identification of a non integer order system, in: ECC, Karlsruhe, Germany, 1999.
[16] C. Lorenzo, T. Hartley, Initialization in fractional order systems, in: 6th European Control Conference, Porto, Portugal, September 2001.
[17] I. Podlubny, Fractional Differential Equations, Academic Press, San Diego, 1999.
[18] K.S. Miller, B. Ross, An Introduction to the Fractional Calculus and Fractional Differential Equations, A Wiley-Interscience Publication, 1993.
[19] M. Aoun, R. Malti, F. Levron, A. Oustaloup, Numerical simulations of fractional systems: An overview of existing methods and improvements, Nonlinear Dynam. 38 (1–4) (2004) 117–131. Special issue: Fractional Derivatives and Their Applications.
[20] D. Matignon, Stability properties for generalized fractional differential systems, in: ESAIM proceedings - Systèmes Différentiels Fractionnaires - Modèles, Méthodes et Applications, 5, 1998.
[21] K.B. Oldham, J. Spanier, The fractionnal calculus, Academic Press, New York and London, 1974.
[22] J.-L. Battaglia, O. Cois, L. Puigsegur, A. Oustaloup, Solving an inverse heat conduction problem using a non-integer identified model, Int. J. Heat Mass Transfer 44 (14) (2001) 2671–2680.
[23] B.M. Vinagre, I. Petras, I. Podlubny, Y.Q. Chen, Using fractional order adjustment rules and fractional order reference models in model reference adaptive control, Nonlinear Dynam. 29 (2002) 269–279.
[24] I. Podlubny, Fractional-order systems and pid controllers, IEEE Trans. Automat. Control 44 (1) (1999) 208–214.
[25] J.A.T. Machado, Analysis and design of fractional-order digital control systems, SAMS Journal of Systems Analysis, Modelling Simul. 27 (1997) 107–122.
[26] R.S. Barbosa, J.A.T. Machado, I.S. Jesus, Fractional pid control of an experimental servo system, in: 3rd IFAC Fractional Differentiation and Its Applications (FDA'08), Ankara, Turkey, November 5–7 2008.
[27] A. Oustaloup, La commande CRONE: du scalaire au multivariable, 2nd edition, Hermès, Paris, 1999.
[28] D. Nelson-Gruel, V. Pommier, P. Lanusse, A. Oustaloup, Robust control system design for multivariable plants with lightly damped modes, in: 21st ASME IDETC/CIE 2007, Las Vegas, USA, September 2007.
[29] A. Oustaloup, La commande CRONE, Hermès, Paris, 1991.